DAB frequency decoupling control with current minimization

Simon UICICH [1,2], Jean-Yves GAUTHIER [1], Xuefang LIN-SHI [1],
Bruno ALLARD [1], Arnaud PLAT [2]
[1] Univ Lyon, INSA Lyon, Universite Claude Bernard Lyon 1, Ecole Centrale de Lyon, CNRS, Ampere, UMR5005,
69621 Villeurbanne, France
E-Mail :jean-yves.gauthier@insa-lyon.fr
[2]AIRBUS OPERATIONS,
26 Chem. de l'Espeissière,
31300 Toulouse, France
E-Mail :arnaud.plat@airbus.com

Keywords

«Dual Active Bridge (DAB)», «Efficiency » «Optimization», «Converter control», «High frequency power converter », «Non-linear control»

Abstract

This paper applies a new Dual-Active-Bridge (DAB) triple-phase-shift (TPS) model modulation to simplify converter analysis, to simplify control and improve efficiency, and reduce transient current stress in the power stage throughout a wide operating space. Achieved current stress is comparable to state-of-the-art. The approach is validated through Simulink-Simscape.

Introduction

The Dual Active Bridge (DAB) is an interesting converter due to the amount of ways in which the phase shifts between its half bridge legs can be controlled to minimize component stress at a given operating condition. Typical modulation approaches achieve this by defining analytical relationships between each phase shift in order to shape inductor current, i.e. triangular current modulation, trapezoidal current modulation (Fig. 1), etc. The goal of this normally achieving low loss (i.e.: minimizing inductor RMS value at given load conditions and achieving certain current values at semiconductor switching instants to guarantee zero voltage switching -ZVS-). In this sense triple-phase-shift (TPS) is the one with the highest potential for optimization since it allows independent control of the phase shift between all 4 half bridges. A typical modulation design approach then uses precise power component loss models for global modulation optimization. Operating space regions are thus matched to modulations, and controllers for each one are developed [1][2]. Straightforward as this is, it has several disadvantages that have been addressed by subsequent research.

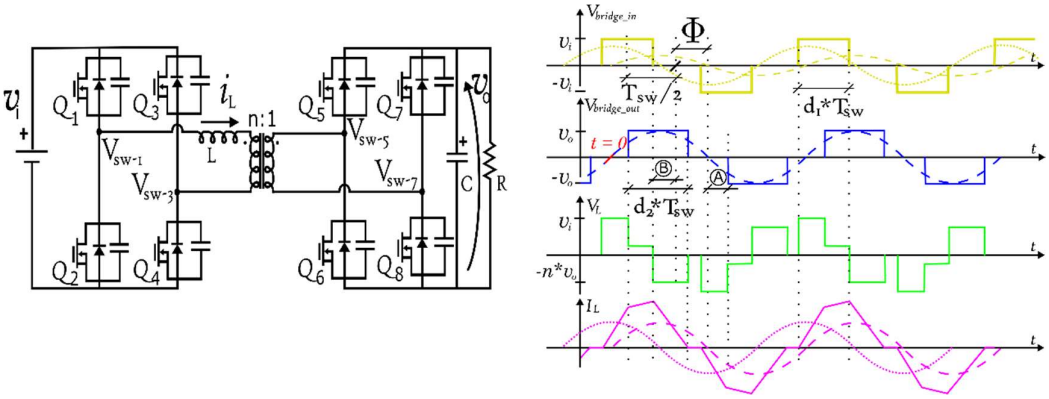

Fig. 1: DAB Schematic and relevant waveforms associated to Triple Phase Shift modulation operation. Relevant wave-forms are $V_{bridge\_in} = V_{sw-} - V_{sw-3}$, $V_{bridge\_out} = V_{sw-5} - V_{sw-7}$, inductor voltage $V_L = V_{bridge\_in} - V_{bridge\_out}$ and current I_L shown in yellow, blue, green and purple respectively. Note: $A = T_{sw}0.5(1 - d_2)$ and $B = T_{sw}0.5(1 - d_1)$

This approach however suffers from design complexity [3][4], design sensitivity to parasitic [5] [6], control variable continuity and output dynamics [1] amongst other issues. Some authors have addressed this. e.g.: with a loss minimization P&O approach to simplify design [7]; optimal approaches for conduction loss min. [8][9] for reduced performance sensitivity and with non-linear approaches limited to low frequency switching operation [10][11] to solve dynamic issues.

Approaching converter control with a generalized multi-frequency averaging approach (MFA) [12][13] avoids these issues. It evaluates the dynamics of frequency components of state space variables through pseudo-Fourier Series coefficients. [14] develops the model for the case of TPS as in [7][9][15] and verifies resemblance to actual circuit behavior. The approach is also found as fundamental component analysis or FCA model in literature[9]. [9]'s approach is similar, but it is restricted to conduction loss reduction ignoring switching loss reduction, and as [16] has shown at low load even this is ineffective due to the FCA model's limited precision. Additionally, neither [17] nor [9] take advantage of the current overshoot prevention, operation with transformer turns ratios bigger than 1 and the possibility of constraining input harmonics which the model can also assess. The stability of the controller is also not guaranteed under large signal state dynamics (small signal modelling). All these disadvantages are the object of the current article's proposed approach.

The paper is organized as follows: Section **FCA model** recalls the DAB fundamental component analysis already developed in the literature. Section **Control Approach** transforms large signal equations to a two-time scale system to facilitate closed-loop control design. Section **Optimisation Strategy** then develops an algorithm based on the model and controller structure aimed to minimize converter RMS current. Section **Validation and Simulation**, verifies the proposed systems performance in Matlab/Simulink, comparing the result to SPS and the state of the art in MFA control. Section **Conclusion** takes stock at the advantages and disadvantages of the presented approach.

FCA model

As underlined previously, the generalized multi-frequency averaging approach can be used to obtain the dynamics of frequency components of state-space variables for the case of TPS modulation. The state-space model obtained is different according to the choice of the time reference and the states. In [9], the reference $t = 0$ is chosen as depicted in Fig. 1. The states used in the model are output voltage average value and transformer current's at the switching frequency, f_{sw}. Then, the FCA model can be expressed as in Eqs. (1) when using in-phase, α, and quadrature, β, fundamental components represented in dashed and dotted lines respectively as in Fig. 1.

$$\frac{dv_0}{dt} = -\frac{v_0}{C \cdot R} + \frac{n}{2\,C} \cdot d_{out,1\alpha} \cdot i_{L,1\alpha} \tag{1.a}$$

$$\frac{di_{L,1\alpha}}{dt} = \frac{v_{in} d_{in,1\alpha}}{L} - \frac{n \cdot v_0 d_{out,1\alpha}}{L} - \frac{R_p \cdot i_{L,1\alpha}}{L} + \omega_0 \cdot i_{L,1\beta} \tag{1.b}$$

$$\frac{di_{L,1\beta}}{dt} = \frac{v_{in} d_{in,1\beta}}{L} - \frac{R_p \cdot i_{L,1\beta}}{L} - \omega_0 \cdot i_{L,1\alpha} \tag{1.c}$$

Where R_p is conduction loss related parasitic resistance, ω_0 given as 2π times f_{sw}, $d_{in,1\alpha}$, $d_{in,1\beta}$, and $d_{out,1\alpha}$, are the fundamental components of the Fourier Series expansion of each full-bridge stages' associated switching function as described by Eqs. (2). In turn, they depend on the actual full order circuit phase shifts d_1, d_2, ϕ as depicted in Fig. 1.

$$d_{in,1\alpha} = \frac{4 \cdot sin(\pi \cdot d_1) \cdot cos(2 \cdot \pi\, \phi)}{\pi} \tag{2.a}$$

$$d_{in,1\beta} = \frac{4 \cdot sin(\pi \cdot d_1) \cdot sin(2\pi \cdot \varphi)}{\pi} \tag{2.b}$$

$$d_{out,1\alpha} = \frac{4 \cdot sin(\pi d_2)}{\pi} \tag{2.c}$$

The FCA model provides information on the response of inductor current, the physical variable used to reduce loss and which impacts switching loss and input harmonics. Thus, it is attractive to develop a control scheme to regulate it, independently of optimization.

Control Approach

The FCA model is a very nonlinear one which can be written as Eqs. (3):

$$\frac{dx}{dt} = f(x,u) \tag{3.a}$$

$$x = [v_0 \quad i_{L,1\alpha} \quad i_{L,1\beta}]^t \quad u = [u_1 \quad u_2 \quad u_3]^t = [d_{out,1\alpha} \quad d_{in,1\alpha} \quad d_{in,1\beta}]^t \tag{3.b}$$

Having a single controller for this model will contribute to system simplification. As [14] shows, model state variable response to a step in one of the control inputs can be divided into two dynamics. A faster one observed in the response of inductor current, and a slower one related to the output capacitor and load response. Thus, the dynamical system of Eq. (1) can be seen as a two-time scale system. A mathematical formalism has been developed for two time-scale systems (corresponding to the so-called "frequency separation" in the linear system framework). The idea is to consider that the dynamic of the slow subsystem is very slow compared to the dynamic of the fast one, i.e. it can be neglected for the fast subsystem control loop design.

The fast time-scale subsystem is composed of the currents $i_{L,1\alpha}$ and $i_{L,1\beta}$.

$$\frac{di_{L,1\alpha}}{dt} = \frac{v_{in}}{L}u_2 - \frac{R_p \cdot i_{L,1\alpha}}{L} + \omega_0 \cdot i_{L,1\beta} - f_1 \tag{4.a}$$

$$\frac{di_{L,1\beta}}{dt} = \frac{v_{in}}{L}u_3 - \frac{R_p \cdot i_{L,1\beta}}{L} - \omega_0 \cdot i_{L,1\alpha} \tag{4.b}$$

Where $f_1 = \frac{n \cdot v_0 d_{out,1\alpha}}{L}$ can be considered as a known disturbance for the current control design.

The slow time-scale system is composed of the output voltage v_0.

$$\frac{dv_0}{dt} = -\frac{v_0}{C \cdot R} + \frac{n}{2\,C} \cdot i_{L,1\alpha}.u_1 \tag{5}$$

Where the dynamic of $i_{L,1\alpha}$ can be neglected to design the voltage control.

This implies two decoupled Linear Time-Invariant (LTI)systems:

- $i_{L,1\alpha}$ and $i_{L,1\beta}$ will be controlled by u_2 and u_3 through Eqs. (4) .
- v_0 can be controlled by u_1 from the 1st order system Eq. (5).

Eqs. (4) lead to expressions for decoupled control while a PI control for Eq. (5) will close the loop for output voltage regulation and create the reference value of $i_{L,1\alpha}$ thus needed. An optimization strategy developed in the next section determines the reference value of $i_{L,1\beta}$ and $u_1(d_{out,1\alpha})$. The next step is then to match each "$u_{1,2,3}$" of the FCA model control space to state variables. It is important to match well to avoid control effort saturating the actual control variables " d_1, d_2, ϕ" – dynamic range between $(-0.5; 0.5)$.

Fig. 2 shows the resulting system diagram. For a given output voltage, two degrees of freedom arise: the reference for $i_{L,1\beta}$ and $d_{out,1\alpha}$. Preliminary simulations showed that the current controller implementation needed to provide transient prevention of saturation in "$\boldsymbol{D}$", for extreme cases. The final part of the control system implementation requires calculating the actual control variables d_1, d_2, ϕ from $d_{in,1\alpha}$, $d_{in,1\beta}$, and $d_{out,1\alpha}$, and using them in a TPS modulator to control Q_1 to Q_8. This is represented by the d_1, d_2, ϕ calculation block from Fig. 2.

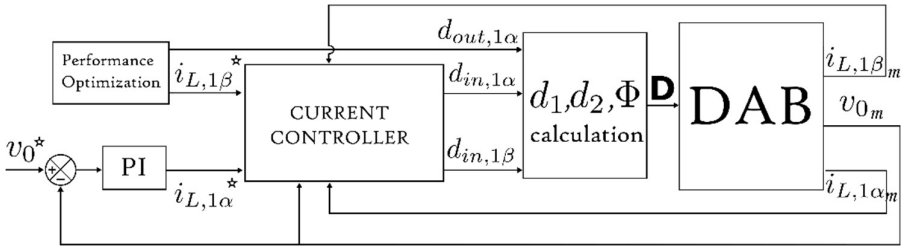

Fig. 2. Block diagram of the proposed control system. Measured values are subscripted with an "m" whereas reference values are marked with a star.

In addition to controlled peak values on power component currents, closed-loop control of $i_{L,1\alpha}$ and $i_{L,1\beta}$ has another key advantage. Namely, if the operating space were divided into regions paired to different optimization approaches – as is normally the case–, approaches which are normally based on current amplitudes, variation of L would not impact the selection of the optimal solution since the controller/optimizer would have this information.

Optimization Strategy

To attract interest, frequency decoupling control should be compatible with classic performance optimization techniques. The classic RMS current minimization problem from [9] is thus first approached. There, it is shown that, for $M = \frac{n*v_o}{v_{in}} < 1$, minimum RMS current is obtained with the control variables from Eqs. (6):

$$d_{out,1\alpha} = d_{out,1\alpha\,\mathrm{MAX}} = \frac{4}{\pi}, \tag{6.a}$$

$$d_{in,1\beta} = \frac{2\,\omega_0\,L\,P}{d_{out,1\alpha}\,v_{in}\,v_0 n} = k_2\,\frac{\pi}{4}, \tag{6.b}$$

$$d_{in,1\alpha}\big|_{k_2 \le \frac{16}{\pi^2}\sqrt{1-M^2}} = \frac{4}{\pi}M \text{ , and} \tag{6.c}$$

$$d_{in,1\alpha}\big|_{k_2 > \frac{16}{\pi^2}\sqrt{1-M^2}} = d_{in,1\alpha\,\mathrm{MAX}} = \frac{16}{\pi^2} - d_{in,1\beta}^2 \tag{6.d}$$

Note that the condition on k_2 equates to a limitation on output power "*P*", with Eq. (6.c) corresponding to low power and Eq. (6.d) corresponding to high power levels. When using the reference from Eq. (6.c) $i_{L,1\alpha}$ is minimized and $i_{L,1\beta} = 0$. In [9], the optimization result showed that minimum RMS current is always obtained, independently of the power level, at $d_{out,1\alpha} = d_{out,1\alpha\,\mathrm{MAX}}$, for $M < 1$. However, it is evident to show that analysis is not valid for $M > 1$. What does still hold from the analysis in [9] for the case of up-conversion though, is that $\min(\mathrm{I_{RMS}})$ can be obtained when $d_{in,1\alpha}^2 + d_{in,1\beta}^2 = \frac{16}{\pi^2}$. Considering Eqs. (7) representing the steady state behavior of Eq. (1):

$$d_{out,1\alpha} i_{L,1\alpha} * n = \frac{2.v_o}{R} = \frac{2P}{v_o} \tag{7.a}$$

$$d_{in,1\beta} = \frac{L\omega_0}{v_{in}} i_{L,1\alpha} = \frac{L\omega_0 2P}{v_o n\, v_{in}\, d_{out,1\alpha}} \tag{7.b}$$

$$i_{L,1\beta} = \frac{1}{L\omega_0}\left(d_{out,1\alpha} n v_0 - v_{in} d_{in,1\alpha}\right) \tag{7.c}$$

If $\mathrm{d_1} = \mathrm{d_{1-MAX}} = 0.5$, Eq. (8) holds. With Eq. (8) and Eq. (7.b) and Eq. (7.a), the steady state value of $i_{L,1\beta}$ can be obtained as in Eq. (9).

$$d_{in,1\alpha}^2 + d_{in,1\beta}^2 = \frac{16}{\pi^2} \tag{8}$$

$$i_{L,1\beta} = \frac{1}{L\omega_0}\left(d_{out,1\alpha} n v_0 - v_{in}\sqrt{\left(\frac{4}{\pi}\right)^2 - \left(\frac{L\omega_0 2P}{v_o n\, v_{in}\, d_{out,1\alpha}}\right)^2}\right) \tag{9}$$

Thus, minimizing RMS current equates to Eq. (10).

$$\min\left(i_{L,1\alpha}^2 + i_{L,1\beta}^2\right) = min\left[\left(\frac{2\,P}{d_{out,1\alpha}\,v_0\,n}\right)^2 + \left(\frac{1}{L\omega_0}\left(nv_o\,d_{out,1\alpha} - v_{in}\sqrt{\left(\frac{4}{\pi}\right)^2 - \left(\frac{L\omega_0 2P}{v_0 n\,v_{in}\,d_{out,1\alpha}}\right)^2}\right)\right)^2\right] \tag{10}$$

With the result for both the FCA model input and $d_{out,1\alpha}$ and state variable $i_{L,1\beta}$ detailed in Eq. (11).

$$d_{out,1\alpha_{opt}} = \sqrt{\left(\frac{\pi P L\omega_0}{2v_{in}v_o n}\right)^2 + \left(\frac{4v_{in}}{\pi v_o n}\right)^2} \tag{11.a}$$

$$i_{L,1\beta_{opt}} = \frac{1}{L\omega}\left(v_o n\,d_{out,1\alpha_{opt}} - v_{in}\sqrt{\left(\frac{4}{\pi}\right)^2 - \left(\frac{L\,\omega_0\,2\,P}{v_o n\,v_{in}\,d_{out,1\alpha_{opt}}}\right)^2}\right) \tag{11.b}$$

The result for other control variables can be immediately derived from Eqs. (7). Here, the fact that $\mathrm{d}_{out,1\alpha} \leq \mathrm{d}_{\mathrm{out},1\alpha\,\mathrm{MAX}} = \frac{4}{\pi}$, implies a limitation on power like the one found for the case of $M < 1$. This can be used to transform the result from Eq. (11.a) and express the constraint as in Eq. (12). If Eq. (12) does not hold, the value of all three d variables is as for the high power case when $M < 1$, i.e.: Eqs. (6.a), (6.b) and (6.d).

$$P \leq \frac{8\,v_{in}v_o n}{\pi^2 L\omega_0}\sqrt{1 - \frac{1}{M^2}} \tag{12}$$

In Fig. 3 both resulting minimum RMS 1st harmonic components are plotted as a function of conversion gain and load. It represents the optimization results here shown, Eqs. (11), and current components obtained with the pre-existing solution for M<1 ([9]). Since the optimization algorithm also needs to generate the $d_{out,1\alpha_{opt}}$reference, it is also included in Fig. 3. It is interesting to note that minimum currents are obtained for low conversion ratios, contrary to [9].

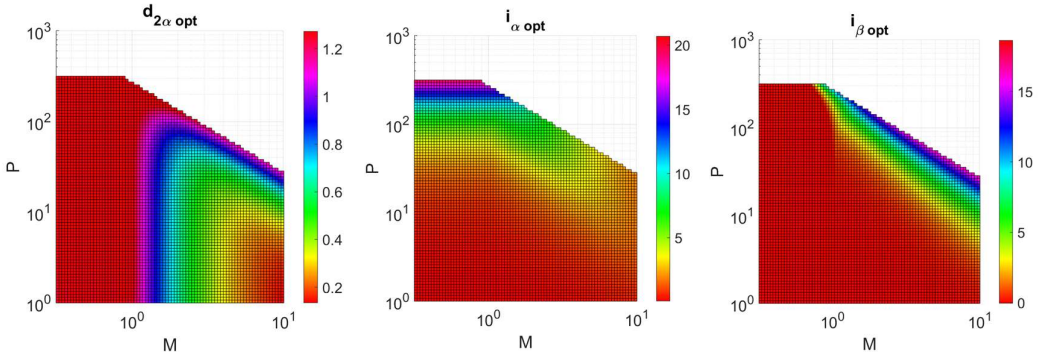

Fig. 3. Result of the optimization analysis for the two current components and $d_{2\alpha}$ variable plotted as a function of conversion ratio and output power. Power is in watts, currents in amperes. Note how higher conversion ratios lead to higher currents at full load.

Simulation Validation

The proposed approach was applied to validate the performance of a 150W, 28V to 12V isolated power supply designed for avionics applications operating at $f_{sw} = 1MHz$ with turns ratio $n = 2$, $L = 0.26uH$ and $C = 3mF$ anr with approximately $R_p = 40m\Omega$ parasitic resistance. It is especially interesting for this type of applications because they involve high v_{in} (between 18V to 46V) and P variation, i.e.: a wide operating range, where typical DAB design struggles to achieve high performances. The simulation was performed on the Simscape full-order converter model of Fig. 4,

with a discrete control frequency, $f_{CONTROL} = f_{sw} = 1MHz$, and 1ns phase shift quantization, a value readily achievable many commercial FPGAs and micro-controllers

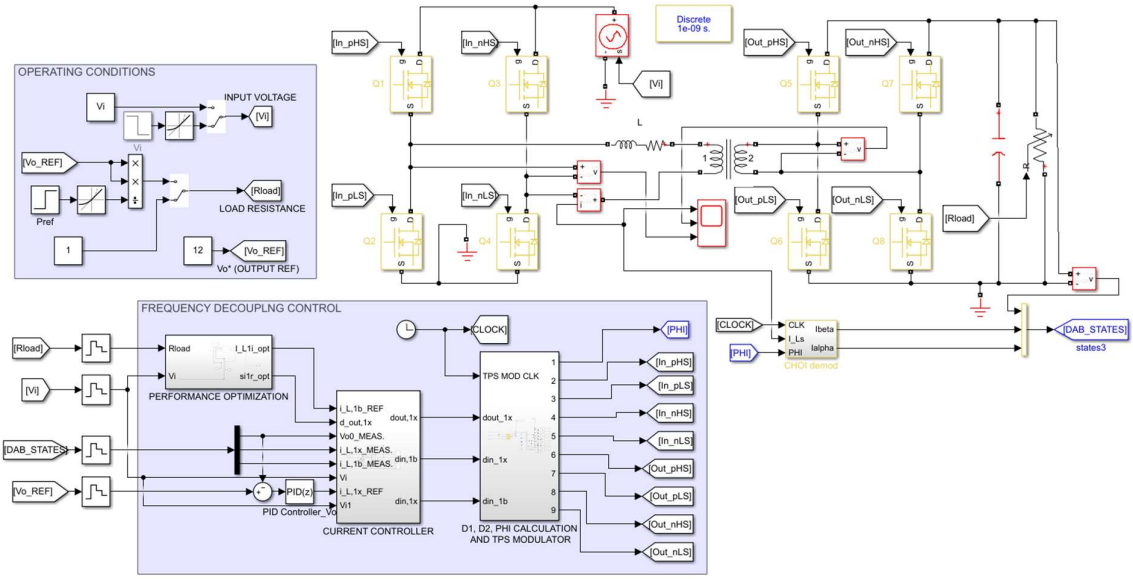

Fig. 4. Schematic of the Simscape model used to validate the proposed control approach. The diagram from Fig. 2 is implemented in the sub-system labelled "FREQUENCY DECOUPLING CONTROL" at the bottom of the image.

From a dynamic performance perspective, with the application covering a wide operating range, one first test that should be performed on the proposed controller structure is to ensure the tracking of state references under operating point variations. Fig. 5 shows control system proper state tracking under a step input voltage variation from minimum to maximum v_i. Note how voltage undershoot as the controller adapts is limited to $100mV$, lasting less than $2ms$.

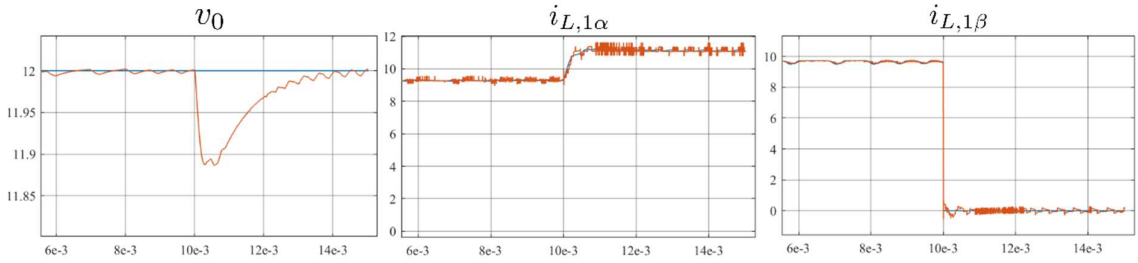

Fig. 5. System's states transient behavior under an input voltage step from 18V to 46V at nominal load. Controller references depicted in blue, state depicted in red. Currents are in amperes, voltages in volts, time is in seconds. The voltage step is applied at $t = 10ms$.

On the other hand, Fig. 6 depicts the proposed approach's inductor current response to a fast load variation. There, a step from 10W to 150W was applied at maximum v_{in}, i.e.: 46V. To highlight the fact that controlled current transitions are guaranteed even if implementing multiple optimization schemes, the proposed optimization scheme was implemented only for power levels above 20% nominal power, i.e. 30W. For power levels below that limit, $i_{L,1\beta}$ and $d_{out,1\alpha}$ references were defined such that steady state current would resemble that of a triangular current modulation scheme as in [2]. Thus, the transition to full power required switching optimization schemes. A smooth current transition can be appreciated, time resolution impeding discerning individual switching periods. The slight overshoot during the beginning of the transient is a DC offset, linked to the way in which phase shifts are updated and is readily avoidable as in [18].

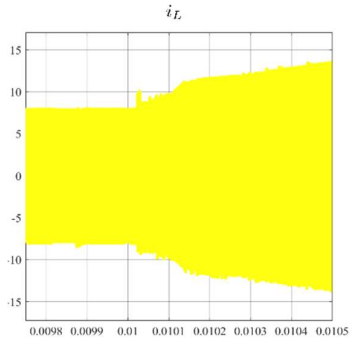

Fig. 6. Transformer current transient behavior under an output load step from 10W to 150W at 46V input voltage. Current is in amperes, time is in seconds. The load step is applied at $t = 10ms$.

Regarding steady state performance, the optimization approach should be able to reduce inductor RMS current in comparison to classical modulation approaches. Fig. 7 shows RMS current values throughout the operating space for both the proposed approach (referenced "FDM", as in "fundamental duty modulation" [9]) and for simple phase shift, noted "SPS". The improvement regarding SPS is considerable, especially in the extremes of the operating region (high/low input voltage), worst case low load and nominal load currents are reduced by more than 60% and 20% respectively.

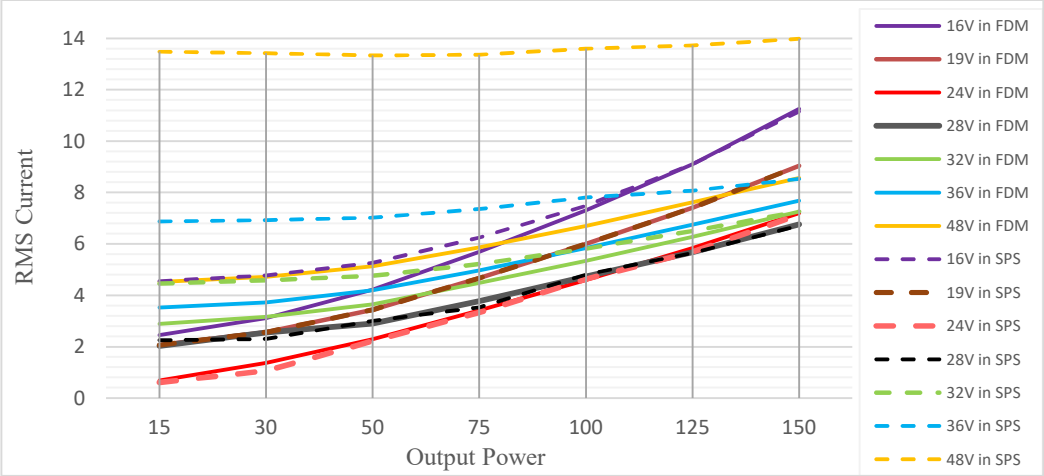

Fig. 7. RMS current throughout the operating range for both the proposed current minimization approach (full lines) vs for SPS (dashed lines). Current represented in amperes, power in watts.

To better evaluate and compare the performance of the current minimization scheme in steady state, the approach from [8] was employed to control the previously described converter under TPS. [8] is a current minimization scheme based on traditional operating mode analysis. RMS currents obtained throughout the operating range are shown in Fig. 8, labelled "TPS". RMS currents obtained when operating under other popular modulation approaches are also represented in Fig. 8. Label "TRM" is for classic triangular current mode [2], where the inductance is charged by v_{in} and then discharged by v_o in a manner similar to a buckboost converter. Currents labelled "Buck" and "Boost" correspond to classic down and up-conversion TRM modulations from [1]. The difference with the one labelled "TRM" being that, for these two, during one of the inductance charge/ discharge phases, the inductance is simultaneously excited by v_{in} and v_o. Analyzing Figs. 7 and 8, it can be concluded that all TRM modulations generate higher RMS currents than the proposed approach throughout the input voltage range at power levels above 20% nominal power, i.e. 30W. On the other hand, the proposed approach generates comparable current levels to the TPS modulation from [8] (less than 10% difference) throughout the input voltage range for power levels above 50% nominal power, i.e. 75W.

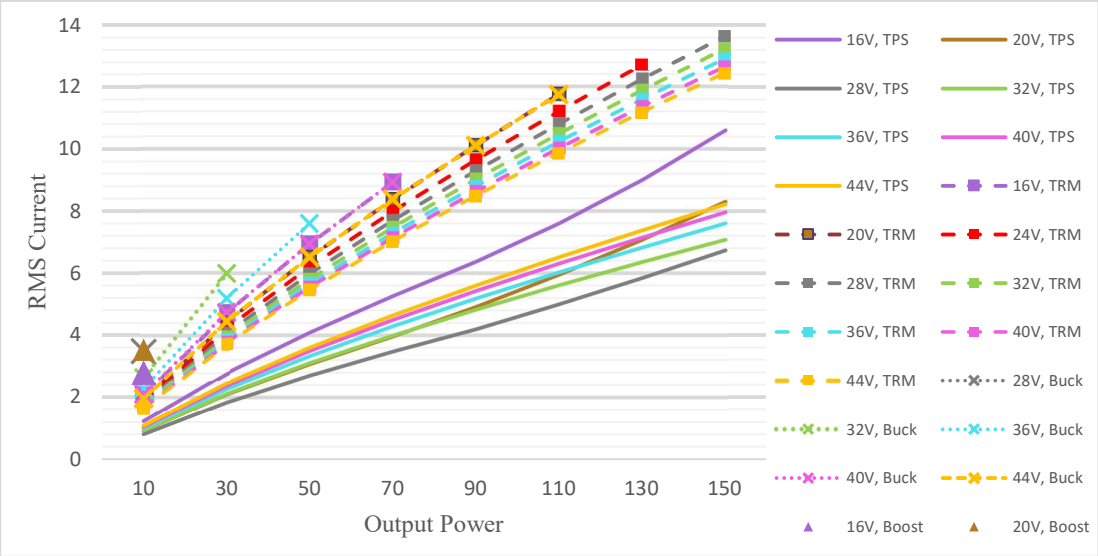

Fig. 8. RMS current throughout the operating range for state of the art ("TPS") and popular TRM modulations ("TRM", "Buck", "Boost") throughout the operating range. Current represented in amperes, power in watts.

Conclusion

A generic control system compatible with triple phase shift modulation was developed. It was shown to provide a simple mechanism to control a DAB converter without the need to analyze operating modes. The current minimization analysis was expanded from [9] to cover M>1 (up conversion). At moderate to high power levels, it was shown to result in RMS currents comparable to state-of-the-art TPS modulations based on operating mode analysis. Transient simulations showed proper tracking of controller references under varying operating conditions and optimization schemes. This shows the approach effectively decoupling optimization from dynamic control of a DAB. Follow up research will demonstrate using the model to reduce input harmonics, further improve converter dynamics and maintain ZVS throughout the load range, even for light load as in [17] and apply the proposed algorithms on a testbench.

References

[1] Krismer F.: Modeling and optimization of bidirectional dual active bridge DC-DC converter topologies, ETH Zurich PhD Thesis 2010.

[2] Yade O.: Commande Prédictive d'un Convertisseur Dual Active Bridge, École Superiéreur Polytéchnique de Dakar, mémoire de fin d'étude, 2015.

[3] Li X.: An Optimized Phase-Shift Modulation For Fast Transient Response in a Dual-Active-Bridge Converter, IEEE Transactions on Power Electronics 29(6):2661-2665

[4] Gu Q.: Current Stress Minimization of Dual-Active-Bridge DC–DC Converter Within the Whole Operating Range, IEEE Journal of Emerging and Selected Topics in Power Electronics, Volume: 7, Issue: 1, pp 129-142

[5] Riedel J.: ZVS Soft Switching Boundaries for Dual Active Bridge DC–DC Converters Using Frequency Domain Analysis, IEEE Transactions on Power Electronics, Vol.: 32, Issue: 4, pp 3166 – 3179

[6] Demumieux P.: Design of a Low-Capacitance Planar Transformer for a 4 kW/500 kHz DAB Converter, 2019 IEEE Applied Power Electronics Conference and Exposition (APEC),

[7] Hebala O.: Generic Closed-Loop Controller for Power Regulation in Dual Active Bridge DC–DC Converter With Current Stress Minimization, IEEE Transactions on Industrial Electronics, Vol.: 66, Issue: 6, pp 4468-4478

[8] Das D.: Optimal Design of a Dual-Active-Bridge DC–DC Converter, IEEE Transactions on Industrial Electronics, Vol.: 68, Issue: 12, pp 12034-12045

[9] Choi W.: Fundamental Duty Modulation of Dual-Active-Bridge Converter for Wide-Range Operation, IEEE Transactions on Power Electronic, Vol.: 31, Issue: 6, pp 4048 – 4064

[10] Oggier G.: Fast transient boundary control of the Dual Active Bridge Converter using the Natural Switching Surface, 2012 IEEE Energy Conversion Congress and Exposition (ECCE)

[11] Takagi K.: Dynamic control and dead-time compensation method of an isolated dual-active-bridge DC-DC converter, 2015 17th European Conference on Power Electronics and Applications (EPE'15 ECCE-Europe)

[12] Caliskan V.A.: Multifrequency averaging of DC/DC converters, IEEE Transactions on Power Electronics, Vol.: 14, Issue: 1

[13] Qin H.: Generalized Average Modeling of Dual Active Bridge DC–DC Converter, IEEE Transactions on Power Electronics, Vol.: 27, Issue: 4

[14] Uicich S.: General DAB 1st Harmonic TPS State Space Model, IECON 2021 – 47th Annual Conference of the IEEE Industrial Electronics Society

[15] Mueller J.A.: An Improved Generalized Average Model of DC–DC Dual Active Bridge Converters, IEEE Transactions on Power Electronics, Vol.: 33, Issue: 11, pp 9975 – 9988

[16] Mou D.: Hybrid Duty Modulation for Dual Active Bridge Converter to Minimize RMS Current and Extend Soft-Switching Range Using the Frequency Domain Analysis, IEEE Transactions on Power Electronics, Vol.: 36, Issue: 4

[17] Mou D.: Five-Degree-of-Freedom Modulation Scheme for Dual Active Bridge DC–DC Converter, IEEE Transactions on Power Electronics, Vol.: 36, Issue: 9

[18] Bu Q.: A Comparative Review of High Frequency Transient DC Bias Current Mitigation Strategies in Dual Active-Bridge DC-DC Converters Under Phase-Shift Modulations, IEEE Trans. Ind. Appl., vol. 58, pp. 2166-2182, December 2021.